# Developing Sub-Domain Verification Methods on GIS Tools

By
Jeffrey A. Smith, Theresa A. Foley, John W. Raby, Brian Reen
U.S. Army Research Laboratory
White Sands Missile Range, NM

## Abstract

The meteorological community makes extensive use of the Model Evaluation Tools (MET) developed by National Center for Atmospheric Research (NCAR) for numerical weather prediction model verification through grid-to-point, grid-to-grid and object-based domain level analyses. MET Point-Stat is used to perform traditional grid-to-point verification. MET Grid-Stat has been used to perform grid-to-grid neighborhood verification to account for the uncertainty inherent in high resolution forecasting, and MET Method for Object-based Diagnostic Evaluation (MODE) has been used to develop techniques for object-based spatial verification of high resolution forecast grids for continuous meteorological variables.

High resolution modeling requires more focused spatial and temporal verification over parts of the domain. With a Geographical Information System (GIS), researchers can now consider terrain type/slope and land use effects and other spatial and temporal variables as explanatory metrics in model assessments. GIS techniques, when coupled with high resolution point and gridded observations sets, allow location-based approaches that permit discovery of spatial and temporal scales where models do not sufficiently resolve the desired phenomena, for example, turbulence effects or mountain and lee waves.

In this paper we discuss our initial GIS approach to verify WRF–ARW with a one-kilometer horizontal resolution inner domain centered near San Diego, California. The San Diego area contains a mixture of urban, sub-urban, agricultural and mountainous terrain types along with a rich array of observational data with which to illustrate our ability to conduct sub-domain verification.

## 1. Introduction

Weather has a significant impact on Army personnel, weapons, tactics and operations; so accurate weather forecasts can be a deciding factor in any conflict large or small. As computing technology advanced, the weather forecasting task, once the primary role of a human forecaster in theater, shifted to computerized Numerical Weather Prediction (NWP) with the human forecaster located far from the area of interest.

Weather forecast validation has always been of interest to the civilian and military weather forecasting community, see for example the reviews by Ebert et al. (2013) and Casati et al. (2008) or the guides by Jolliffe and Stephenson (2011) or Wilks (2011). Along with the development of increasingly powerful computing technology, interest in validation shifted from the accuracy of human forecasters to the accuracy of the NWP models. The validation of the models, especially high resolution models produced by NWP, has proven to be especially difficult when addressing small time and spatial scales (National Research Council 2010).

The numerical weather prediction community continues to pursue the development of high resolution NWP codes as typified by the current implementation of the Advanced Research version of the Weather Research and Forecasting (WRF) (WRF–ARW; Skamarock et al. (2008)) model that utilizes Four Dimensional Data Assimilation (FDDA) techniques (Stauffer and Seaman 1994; Deng et al. 2009). The U.S. Army Research Laboratory (ARL) is using WRF-ARW as the core of its Weather Running Estimate – Nowcast (WRE–N) to investigate methods of ingesting weather observations via FDDA to improve the quality of the forecasts. To show where and how FDDA adds value, we need a means to compare battlefield nowcasts produced with FDDA to those produced without FDDA. By comparing these forecasts over the domain using more traditional tools, and spatial and temporal comparisons over sub-domains using other tools, we expect that we can quantify the potential benefits as well as identifying the means to improve our FDDA approach. (Raby et al. 2012)

In prior model assessments, ARL employed the Model Evaluation Tools (MET) (NCAR 2013) developed by the National Center for Atmospheric Research (NCAR) Developmental Testbed Center (DTC) for use by the numerical weather prediction community, especially users and developers of the WRF model, to help them assess and evaluate the performance of the models. One such example assessment is that of Raby et al. (2012) who evaluated two models to arrive at domain level conclusions about the various strengths and weaknesses of these models and their accuracies. While MET proved useful as an assessment tool for forecasts over a regional domain, we found its ability to illuminate model short comings on the spatial and temporal scales needed by battlefield commanders to be lacking.

In another assessment Dumais et al. (2012) evaluated three models that produced three-dimensional wind fields to arrive at domain level conclusions. Though Dumais et al. did not

employ any of the MET tools in their analysis; their desire was to identify model strengths and weaknesses. Again, they found their ability to draw spatial and temporal conclusions lacking.

To conduct our investigation, we employed a domain located in the San Diego, California region to assess the ability of Geographic Information Systems (GIS) tools and techniques to enhance model verification. For our study, we used the MET tool "Point-Stat" which generates data for grid-to-point verification, or verification of a gridded forecast field against point-based observations (i.e., surface observing stations, rawinsondes, and other point observations). It provides forecast verification scores for both continuous (e.g., temperature) and categorical (e.g., rain) variables with associated confidence intervals. Confidence intervals take into account the uncertainty associated with verification statistics due to sampling variability and sample size limitations. Specifically, we analyzed the matched forecast-observation pair output of Point-Stat using a GIS to expand the analysis of the WRE–N/FDDA output and point observations within an extremely high resolution terrain framework.

Our assertion (Smith et al. 2013; Smith et al. 2014) is that high-resolution models require verification on temporal and spatial scales appropriate for the phenomenon that are being forecast. The atmospheric flows of interest are mountain/valley breezes, sea breezes and other flows induced by differences in land surface characteristics. The traditional verification approach used by Point-Stat aggregates the error statistics over the entire domain, techniques which produce results that often appear smoothed because of averaging and consequently may not show the value added of higher resolution Nowcast output at grid resolutions of 1km or less. More in-depth analysis of the forecast errors are needed to deduce the various sub-regimes, temporal and spatial trends which may govern the statistics in a way which cannot be seen when the statistics are aggregated over the entire domain. Our principal thesis is that GIS tools may allow us to break the domain into sub-domains according to variables such as terrain and land use; sub domains whose data are more homogeneous and consequently more amenable to accurate inferences about model performance as well as providing a better understanding of model strengths and weaknesses.

## 2. Domain and Model

The ARL WRE–N (Dumais et al. 2004; Dumais and Reen 2013) has been designed as a convection-allowing application of the Advanced Research version of the Weather Research and Forecast (WRF–ARW) model (Skamarock et al. 2008) and its observation nudging FDDA option (Liu et al. 2005; Deng et al. 2009). For this investigation, we configured WRE–N in a multi-nest configuration to produce a fine inner mesh of around 1 km grid spacing (i.e.; 9 /3 /1 km) and leveraged an external global model for cold-start initial conditions and time-dependent lateral boundary conditions for the outermost nest. For ARL development and testing, this global model has been the National Center for Environmental

Prediction's Global Forecast System (GFS) model (Environmental Monitoring Center 2003). The WRE–N is essentially a rapid-update cycling application of WRF–ARW with FDDA, and optimally can refresh itself at intervals up to hourly (dependent upon the observation network) (Dumais et al. 2012; Dumais and Reen 2013).

For this particular experiment, the model was run with a base time of 1200 UTC and generated 24 hourly outputs for five days in February and March of 2012. The modeling domain is depicted in Figure 1.

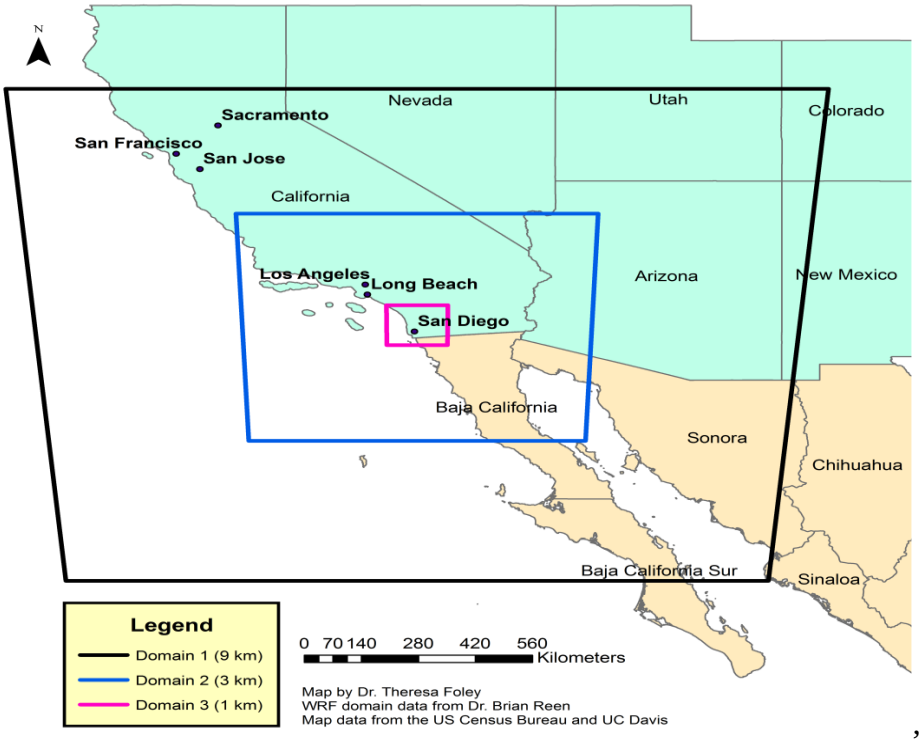


**Figure 1: Triple-nested configuration with an outer nest mesh of 9km (1566 km by 1566 km); the middle nest mesh of 3km (720 km by 720 km); and, the inner nest mesh of 1km spacing (126 km by 126 km) centered over Southern California near San Diego.**

The initial conditions were constructed by starting with the GFS data as the first-guess for an analysis using observations. Most observations were obtained from the Meteorological Assimilation Data Ingest System (MADIS) (2014) except that the Tropospheric Airborne Meteorological Data Reporting (TAMDAR) observations were obtained from AirDat (2014). The MADIS observations included standard surface observations, mesonet surface observations, maritime surface observations, wind profiler measurements, rawinsonde soundings and ACARS aircraft data. Use and reject lists obtained from developers of the Real-Time Mesoscale Analysis (2014) system and were used to filter MADIS mesonet observations; this is especially important given the greater tendency of mesonet observations to be poorly sited than other, more standard, surface observations. The WRF component Obsgrid was used to quality control all observations; this included gross error checks, comparing observations to a background field (here GFS), and comparing observations to

nearby observations. Obsgrid was modified to allow single-level observations, like the TAMDAR and ACARS aircraft data used here, to be more effectively compared against the background field (GFS). Observation nudging is applied using observations from these same sources from 1200 to 1800 UTC, followed by one-hour ramping down of the nudging from 1800 to 1900 UTC during which time no new observations are assimilated; consequently, 1800 UTC begins the forecast period since no observations after this time are assimilated.

For the physical parameterizations of the WRE–N , a modified version of the Mellor–Yamada–Janjić (MYJ) Planetary Boundary Layer (PBL) (Janjić 1994) scheme was used. This modification decreases the background turbulent kinetic energy (TKE) and alters the diagnosis of PBL depth used for model output and data assimilation. The WRF single-moment, 5-class microphysics parameterization is used on all domains (Hong et al. 2004), while the Kain-Fritsch (Kain 2004) cumulus parameterization is used only on the 9-km domain. For radiation, the RRTM (Mlawer et al. 1997) is used for longwave and Dudhia (Dudhia 1989) scheme for shortwave. The Noah land surface model is used (Chen and Dudhia 2001a, 2001b). Additional references and other details for these parameterization schemes are available from Skamarock (2008).

The case study days were selected on the basis of the prevailing synoptic weather conditions over the nested domains, and a short description of these conditions is provided in Table 1.

**Table 1: Synoptic conditions for the case study days considered**

| Case | Dates (all 2012) | Description |
|---|---|---|
| 1 | February 07–08 | Upper level trough moved onshore which led to widespread precipitation in the region. |
| 2 | February 09–10 | Quiescent weather was in place with a 500-hPa ridge centered over central California at 12 UTC. |
| 3 | February 16–17 | An upper level low is near the California/Arizona border with Mexico at 12 UTC, bringing precipitation to that portion of the domain. This pattern moved south and east over the course of the day. |
| 4 | March 01–02 | A weak shortwave trough results in precipitation in northern California at the beginning of the period that spreads to Nevada, and then moves southward and decreases in coverage. |
| 5 | March 05–06 | Widespread high-level cloudiness due to weak upper level low pressure but very limited precipitation. |

After model execution and generation of the Point-Stat matched pair output, with duplicate handling set to SINGLE so that we only report a single matched pair per hour for each observation station, we conducted a quality control analysis of the forecast and observation data, focusing our attention on surface observations (2 meter above ground level (AGL) temperature and moisture, and 10 meter AGL wind). We did not consider several observation stations reporting from different mesonets with a common site id. These sites reported with different latitude and longitude and/or elevations depending on the particular mesonet the data came from, and these differences resulted in reports being in some cases a kilometer or more apart. However, this reduction in number of stations was not an appreciable loss in observational data. Once we completed our quality control, we further restricted our attention to only those stations that reported observations in each of the 25 hours of a given case day (1200 UTC from the beginning to 1200 UTC at the end). Our intent in making this restriction was twofold: 1) we could make hour to hour comparisons using the same base set of data, and 2) any remaining stations within a given hour would serve as means to cross-validate our analysis. The number of stations considered for each case day is given as Table 2. Note that here we only describe statistics from the 2-m AGL temperature and moisture and not on the 10-m AGL wind statistics.

**Table 2: Count of stations that were used in each case study by case and altitude above ground level (AGL); for two meters, these were stations reporting the Temperature and moisture data, and for 10 meters, these were stations reporting wind.**

| | Altitude (AGL) | |
|---|---|---|
| Case | 2 meters | 10 meters |
| 1 | 135 | 72 |
| 2 | 96 | 48 |
| 3 | 122 | 58 |
| 4 | 133 | 80 |
| 5 | 69 | 47 |

## 3. Results

We used ESRI's ArcGIS for Desktop (ESRI 2014) to geo-locate the Point-Stat matched pair data consisting of observing station location, elevation, value of observed meteorological variable and the value of the forecast variable interpolated to the station location within the 1/3 arcsec resolution digital elevation model (DEM) framework (U.S. Geological Survey 2013). We depict the geo-located stations we used in our analysis of case day 1 in Figure 2.

In our analysis of the first case day, we studied the five specific hours given in Table 1. We chose these specific times to examine the impact of the data assimilation and subsequently the forecasts. In the analysis that follows, we look at the forecasts for February 7-8, 2012 specifically for the 0600 and 1200 UTC times that roughly corresponding to early stable planetary boundary layer formation and late stable boundary layer conditions.

We computed bias errors for all observation stations, defined as the forecast value minus the observed value, for each meteorological variable (temperature, relative humidity, and dew point) at the Z2 surface level corresponding to two meters AGL. Note that the model 2-m diagnostic temperature and moisture values were used as the forecast values. Over the domain, our analysis showed that we could treat these bias errors as Gaussian. Consequently we treated each bias error as a sample point from a random field, and employed the "Empirical Bayesian Kriging" (EBK) (Krivoruchko 2011, 2012) feature of ArcGis to estimate a continuous surface for the point forecast error data. Note that these surfaces will not extend to the western or southern extents of the domain because there is insufficient data in these areas to produce a statistically significant surface estimate.

Inspection of these error surfaces for the dew point and relative humidity variables showed that the distribution of these errors were in reasonable spatial agreement with one another at 2 meters AGL; therefore, we focused our attention on the two directly measured variables temperature and relative humidity instead of the derived variable dew point.

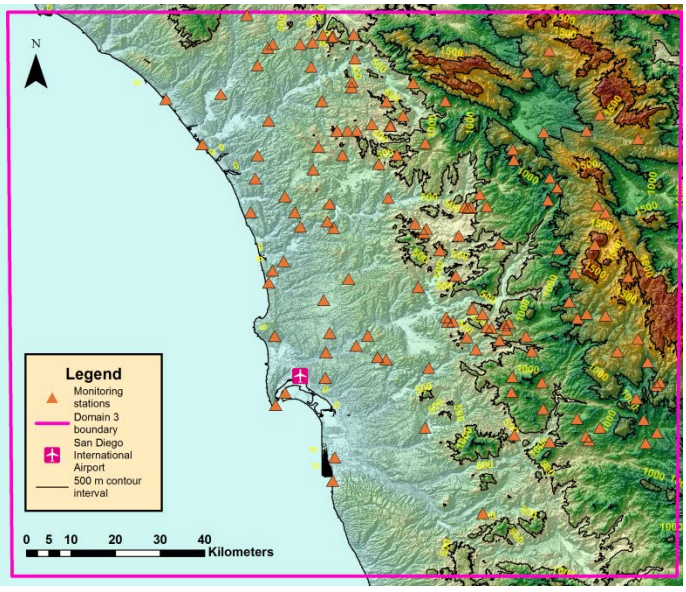


**Figure 2: Geo-located observations stations reporting temperature data used in case day 1 analysis for the inner, 1 km grid spacing, nest (Domain 3). Each station is indicated by a single triangle.**

To gauge model performance, we employed MET to compute the matched pair statistics over the inner, one kilometer grid spacing, domain (domain 3). The domain aggregate statistics

are presented as Table 4. These statistics indicate that at the domain level, the model performed well over the forecast period with unremarkable errors.

**Table 3: Analysis times and rationale for choice**

| Period | Time (hr) | | | Reason |
|---|---|---|---|---|
| | UTC | Forecast Lead | Local (PST) | |
| Assimilation | 1200 | 0 | 0400 | Beginning of data assimilation |
| | 1800 | 6 | 1000 | End of data assimilation |
| Forecast | 0000 | 12 | 1600 | Late afternoon, unstable PBL |
| | 0600 | 18 | 2200 | Early evening, slightly stable PBL |
| | 1200 | 24 | 0400 | Early morning, stable PBL |

Our next step was to employ EBK to estimate surfaces of the forecast error for the two forecasted variables: temperature (Figure 3) and relative humidity (Figure 4). Our intent with this analysis was to explore the model bias errors spatially to identify potential geographic variables such as elevation, distance from the coast, and slope that would allow us to more thoroughly explore these errors.

**Table 4: Mean errors of the bias (forecast - observed) errors for each of the five case days, and at each of the three meteorological variables present at the Z2 surface level (two meters AGL) at 4 PM PST (0000 UTC) and 4 AM PST (1200 UTC) for next day in the case.**

| Case | UTC | Temperature (K) | Dew Point (K) | Relative Humidity (%) |
|---|---|---|---|---|
| 1 | 0000 | −0.17 | 1.11 | 5.83 |
| | 1200 | 0.76 | 1.40 | 2.39 |
| 2 | 0000 | −2.89 | 2.95 | 12.27 |
| | 1200 | 2.42 | −1.35 | −13.76 |
| 3 | 0000 | −0.65 | 0.09 | 1.94 |
| | 1200 | 0.81 | −2.18 | −11.31 |
| 4 | 0000 | 0.30 | 0.23 | 0.14 |
| | 1200 | 1.58 | −2.18 | −18.66 |
| 5 | 0000 | −3.55 | 3.48 | 17.34 |
| | 1200 | −0.13 | −0.59 | −1.57 |

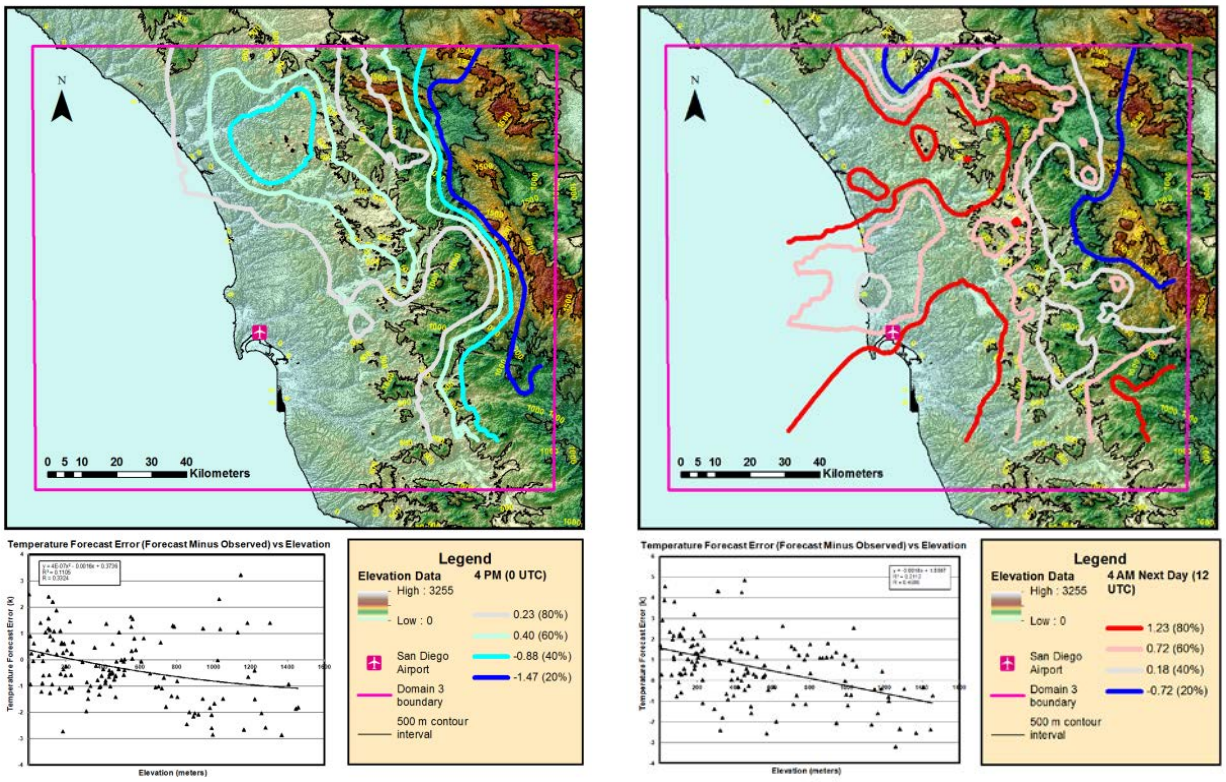


**Figure 3: (a) Upper left image is a contour plot of the estimated surface for the temperature error bias at 0000 UTC (4 PM PST, 07 February 2012). Each line of the contour is a quintile of the error surface. The surface tends from a 0.23K upper quintile along the coast, to a -1.47K lower quintile over the mountains east of San Diego. (b) Lower left scatter plot of the temperature error bias versus elevation, showing some significant outliers, with a least square regression estimated second order polynomial, but with only a very small quadratic component; however, the Pearson correlation coefficient is not statistically significant possibly because the boundary layer is unstable. (c) Upper right image is a contour plot of the estimated surface for the temperature error bias at 1200 UTC (4 AM PST, 08 February 2012). Each line of the contour is a quintile of the error surface. The surface tends from a 1.23K upper quintile along the coast, to a -0.72K lower quintile over the mountains east of San Diego. (d) Lower right scatter plot of the temperature error bias versus elevation with a least square regression estimated first order polynomial. For this polynomial, the Pearson correlation coefficient is statistically significant at 0.46 possibly because the planetary boundary layer is more stable.**

We generally observed that the tendency to over or under forecast both temperature and relative humidity seemed to be related to the elevation of the observation station. To investigate this, we partitioned the data into two parts via a threshold value that ranged from 200 to 1000 meters above sea level in elevation. We used this simple method to explore Pearson's correlation coefficient for the temperature versus elevation data that lay above and below this threshold, with a goal of finding a partition elevation of the surface temperature data that would maximize the correlation coefficient on both sides of the threshold; however, this analysis was inconclusive. For the 4 PM PST time (0000 UTC), when the threshold was 400 meters or above, we observed statistically significant (at an alpha of 0.10) weak to moderate correlations (-0.17 to -0.43) for all temperature versus elevation comparisons below the 400, 500, …, 1000 meters above sea level thresholds; however, the comparisons above

that same threshold were mixed significant and non- significant correlations with no obvious trend. For the 4 AM PST time (1200 UTC), at every threshold value we had statistically significant correlation coefficients for moderate correlations (-0.27 to -0.64) both above and below the threshold.

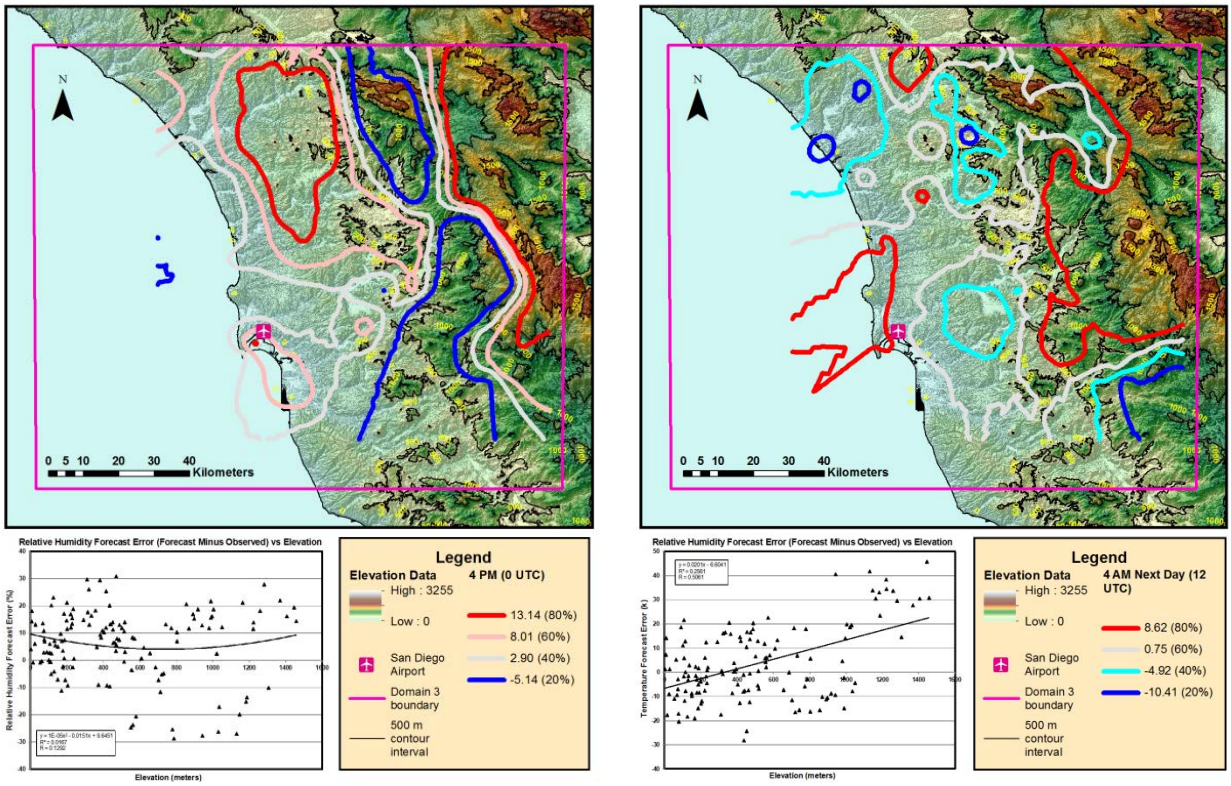


**Figure 4: (a) Upper left image is a contour plot of the estimated surface for the relative humidity error bias at 0000 UTC (4 PM PST, 07 February 2012). Each line of the contour is a quintile of the error surface. The surface tends from a 13.14% upper quintile to the north and along the mountains east, of San Diego to a 5.14% lower quintile along the mountain slopes east of San Diego. (b) Lower left scatter plot of the temperature error bias versus elevation, showing some significant outliers, with a least square regression estimated second order polynomial, but with only a very small quadratic component; however, the Pearson correlation coefficient is not statistically significant possibly because the boundary layer is unstable. (c) Upper right image is a contour plot of the estimated surface for the relative humidity error bias at 1200 UTC (4 AM PST, 08 February 2012). Each line of the contour is a quintile of the error surface. The surface tends from an 8.62% upper quintile to the north, and along the mountains east, of San Diego to a -10.41% lower quintile scattered over the coastal areas and the south end of the mountains. (d) Lower right scatter plot of the temperature error bias versus elevation, showing some significant outliers and a least square regression estimated first order polynomial. For this polynomial, the Pearson correlation coefficient is statistically significant possibly because of a more stable planetary boundary layer.**

## 4. Conclusions

At this stage, the results demonstrate that we have developed a method to analyze spatially distributed point forecast errors using a GIS. Using the tools of the GIS, the errors can be analyzed to show the possible dependence on terrain characteristics at the spatial scales of phenomena of interest to Army warfighters such as mountain/valley breezes and land/sea breezes which are themselves tied to the local terrain variables. The employment of statistical analysis and the results obtained from this work show considerable promise toward the goal of demonstrating the relationships and dependencies of high resolution forecast errors to terrain characteristics in sub-domains where the statistics are more homogeneous. Although, the analysis results show interesting spatial trends in the errors, further analysis will be needed to draw firm conclusions about the performance of the WRE–N/FDDA. Our goal, which was to develop a method to go beyond the types of conclusions gained from domain-level, aggregate statistics was achieved.

## 5. Acknowledgements

We offer our thanks to Mr. Jeff Passner, Dr. Huaqing Cai, Dr. Richard Penc, LTC John Olson, Ph.D., and Mr. Jeff Johnson. Each of these individuals contributed to our work in varying degrees, and without their feedback we would not have progressed as far as we did.

References

AirDat, cited 2014: AirDat Real-Time TAMDAR Weather Data and Products. [Available online at http://www.airdat.com/.]

Casati, B., and Coauthors, 2008: Forecast verification: current status and future directions. *Meteorological Applications*, **15,** 3-18.

Chen, F., and J. Dudhia, 2001a: Coupling an advanced land surface-hydrology model with the Penn State-NCAR MM5 modeling system. Part I: Model implementation and sensitivity. *Monthly Weather Review*, **129,** 569-585.

——, 2001b: Coupling an advanced land surface-hydrology model with the Penn State-NCAR MM5 modeling system. Part II: Preliminary model validation. *Monthly Weather Review*, **129,** 587-604.

Deng, A., and Coauthors, 2009: Update on the WRF-ARW end-to-end multi-scale FDDA system. *10'th WRF Users' Workshop*, National Center for Atmospheric Research, paper 1.9.

Dudhia, J., 1989: Numerical study of convection observed during the Winter Monsoon Experiment using a mesoscale two-dimensional model. *J Atmos Sci*, **46,** 3077-3107.

Dumais, R. E., and B. P. Reen, 2013: Data assimilation techniques for rapidly relocatable weather research and forecasting modeling. Final Report ARL-TN-0546.

Dumais, R. E., J. W. Raby, Y. Wang, Y. R. Raby, and D. Knapp, 2012: Performance assessment of the three-dimensional wind field Weather Running Estimate-Nowcast and the three-dimensional wind field Air Force Weather Agency weather research and forecasting wind forecasts. Technical Note ARL-TN-0514.

Dumais, R. E., Jr., T. Henmi, J. Passner, T. Jameson, P. Haines, and D. Knapp, 2004: A mesoscale modeling system developed for the U.S. Army. Final Report ARL-TR-3183.

Ebert, E., and Coauthors, 2013: Progress and challenges in forecast verification. *Meteorological Applications*, **20,** 130-139.

Environmental Monitoring Center, 2003: The GFS Atmospheric Model. NCEP Office Note 442.

ESRI, 2014: ArcGIS 10.2: ArcGIS for Desktop with ArcGIS Geostatistical Analysis, Spatial Statistics and 3D Analysis Toolboxes. Environmental Systems Research Institute, Inc.

Hong, S.-Y., J. Dudhia, and S.-H. Chen, 2004: A revised approach to ice microphysical processes for the bulk parameterization of clouds and precipitation. *Monthly Weather Review*, **132,** 103-120.

Janjić, Z. I., 1994: The step-mountain eta coordinate model: Further developments of the convection, viscous sublayer, and turbulence closure schemes. *Monthly Weather Review*, **122,** 927-945.

Jolliffe, I. T., and D. B. Stephenson, 2011: *Forecast verification: A practitioner's guide in atmospheric science.* 2nd ed. John Wiley & Sons.

Kain, J. S., 2004: The Kain-Fritsch convective parameterization: An update. *Journal of Applied Meteorology*, **43,** 170-181.

Krivoruchko, K., 2011: *Spatial statistical data anlysis for GIS users.* ESRI Press, 928 pp.

——, 2012: Empirical Bayesian kriging: Implemented in ArcGIS Geostatistical Analyst. *ArcUser*, **15,** 6-10.

Liu, Y., A. Bourgeois, T. Warner, S. Swerdlin, and J. Hacker, 2005: Implementation of observation-nudging based FDDA into WRF for supporting ATEC test operations. *The 6th WRF/15th MM5 Users' Workshop*, National Center for Atmospheric Research.

Mlawer, E. J., S. J. Taubman, P. D. Brown, M. J. Iacono, and S. A. Clough, 1997: Radiative transfer for inhomogeneous atmospheres: RRTM, a validated correlated-k model for the longwave. *Journal of Geophysical Research-Atmospheres*, **102,** 16663-16682.

National Center for Atmospheric Research, 2013: Model Evaluation Tools Version 4.1 (METv4.1). User's Guide 4.1.

National Oceanic and Atmospheric Administration (NOAA) Global Systems Division (GSD), cited 2014: Meteorological Assimilation Data Ingest System (MADIS). [Available online at http://madis.noaa.gov/.]

National Oceanic and Atmospheric Administration (NOAA) National Center for Environmental Prediction (NCEP), cited 2014: Real-Time Mesoscale Analysis (RTMA). [Available online at http://www.nco.ncep.noaa.gov/pmb/products/rtma/.]

National Research Council, 2010: *When weather matters: Science and service to meet critical societal needs.* The National Academies Press.

Raby, J., J. Passner, G. Vaucher, and Y. Raby, 2012: Performance comparison of high resolution weather research and forecasting model output with north american mesoscale model initialization grid forecasts. Final Report ARL-TR-6000.

Skamarock, W. C., and Coauthors, 2008: A description of the advanced research WRF version 3. NCAR Technical Note NCAR/TN-475+STR.

Smith, J. A., J. Raby, and T. Foley, 2013: Comparing high resolution weather forecasts to observations. *Fall Meeting of the American Geophysical Union.*

Smith, J. A., T. A. Foley, and J. W. Raby, 2014: Developing sub-domain verification methods based on GIS tools. *15'th WRF Users Workshop*, Boulder, CO.

Stauffer, D. R., and N. L. Seaman, 1994: Multiscale four-dimensional data assimilation. *Journal of Applied Meteorology*, **33,** 416-434.

U.S. Geological Survey, 2013: Digital Elevation Model.

Wilks, D. S., 2011: *Statistical methods in the atmospheric sciences.* 3rd ed. Academic Press.